ELSEVIER

Journal of the Mechanics and Physics of Solids
52 (2004) 755–787

JOURNAL OF THE
MECHANICS AND
PHYSICS OF SOLIDS

www.elsevier.com/locate/jmps

Multiscale plasticity modeling: coupled atomistics and discrete dislocation mechanics

L.E. Shilkrot[a,1], Ronald E. Miller[b,*], William A. Curtin[a]

[a] *Division of Engineering, Brown University, Providence, RI, 02912, USA*
[b] *Department of Mechanical and Aerospace Engineering, Carleton University, Ottawa, ON, K1S 5B6, Canada*

Received 10 April 2003; received in revised form 8 September 2003; accepted 11 September 2003

Abstract

A computational method (CADD) is presented whereby a continuum region containing dislocation defects is coupled to a fully atomistic region. The model is related to previous hybrid models in which continuum finite elements are coupled to a fully atomistic region, with two key advantages: the ability to accomodate discrete dislocations in the continuum region and an algorithm for automatically detecting dislocations as they move from the atomistic region to the continuum region and then correctly "converting" the atomistic dislocations into discrete dislocations, or vice-versa. The resulting CADD model allows for the study of 2d problems involving large numbers of defects where the system size is too big for fully atomistic simulation, and improves upon existing discrete dislocation techniques by preserving accurate atomistic details of dislocation nucleation and other atomic scale phenomena. Applications to nanoindentation, atomic scale void growth under tensile stress, and fracture are used to validate and demonstrate the capabilities of the model.

Keywords: Multiscale modelling; Atomistic simulation; Dislocations; Atomistic continuum coupling

1. Introduction

There are many problems in materials science for which physical phenomena occurring at several length and/or time scales are relevant to properly understanding the material behavior. One class of such problems is the deformation and ultimate

* Corresponding author. Tel.: +1-61-35202600; fax: +1-61-35205715.
E-mail address: rmiller@mae.carleton.ca (R.E. Miller).

[1] Current Address: Argonne National Laboratory, 9700 S. Cass Ave., Argonne IL 60439.

0022-5096/$ - see front matter © 2003 Elsevier Ltd. All rights reserved.
doi:10.1016/j.jmps.2003.09.023

failure of ductile metals, where cracks, grain boundaries and large numbers of mobile dislocations undergo complex interactions. At the smallest scale of Angstroms, details of the dislocation core structures and mechanisms of their nucleation and motion can profoundly affect the macroscopic response of the crystal. At the same scale, crack growth, driven by high loading, chemical embrittlement, or fatigue, requires actual material separation that is highly non-linear and not amenable to simple descriptions at larger scales. However, elastic interactions between defects at distances of micrometers or more lead to effects such as crack tip shielding by dislocations, dislocation patterning, dislocation pile-ups at grain boundaries and other deformations that contribute significantly to macroscopic strength, ductility and toughness.

Direct atomistic simulation of material response is often not feasible. At the present state of the art, direct atomistic simulations can typically consider hundreds of thousands of atoms, corresponding to a block of material having characteristic dimensions of approximately 0.1 μm. A typical grain size in metals may be as small as 10 μm, so clearly the length scale amenable to atomistic modeling is well below the range required for modeling realistic microstructures. Furthermore, plastic zone sizes in ductile metals can be anywhere from micrometers to millimeters, and hence atomistic methods alone can never achieve the necessary scales. In fact, much of the information obtained from direct large-scale atomistic simulations is excessive and unnecessary. The goal of a simulation is to focus on regions of the material containing "interesting" physics where atom are significantly displaced from lattice sites or have coordination numbers different from those of the perfect lattice. A parameter used to identify such atoms is the deviation of the individual atom energy from the average atom energy. Results from gigantic atomistic simulations (1 billion atoms) show (Abraham, et al., 2002) that the high-energy atoms are clustered around microstructural defects such as cracks or grain boundaries or form threads of intermingled dislocation lines and are a small percentage of the total. The energies of the majority of atoms are around the average; these atoms have small displacements and, therefore, are amenable to a continuum description. One would naturally want to exclude these atoms from burdensome atomistic computations.

Multiscale methods of modeling plasticity and ductile fracture usually fall under one of two possible categories. One approach is hierarchical: physical phenomena occurring at different scales are modeled separately and behavior of the system at the smaller scales is used as a source of parameters that enter more-phenomenological descriptions at the larger scales. This approach is typified in the recently developed discrete dislocation (DD) techniques (Kubin and Canova, 1992; van der Giessen and Needleman, 1995; Zbib et al., 1998) of particular interest here, wherein dislocations are treated as continuum entities moving in fields determined by elasticity. The long range interactions between the defects are thus modeled accurately while smaller-scale phenomena and short-range dislocation interactions are described by a set of constitutive rules. The rules dictate, for instance, the conditions required for dislocation nucleation, the minimum dislocation separation for annihilation, the strength of dislocation junctions, the dislocation mobility, and dislocation/obstacle interactions. Suitable values for the parameters in these rules can be obtained, in principle, through small, detailed atomistic simulations. However, the myriad of possible complex atomistic interactions makes a full description difficult.

The second approach to multiscale modeling is represented by hybrid schemes that model some spatial regions of a problem using a fully atomistic approach and other regions using a continuum scheme. The FEAt method of Kohlhoff et al. (1991) and the CLS approach of Rudd and Broughton (2000) achieve this hybrid coupling using linear elastic finite elements. However, these approaches do not support continuum dislocations in the finite element region, nor can they easily adapt the size of the atomistic region during the simulation. The quasicontinuum (QC) method of Shenoy et al., 1998; Tadmor et al. (1996) makes use of a special finite element in the continuum region whose constitutive law is based on the response of a small representative crystallite of atoms to the local continuum deformation field. This approach ensures that, in the limit of atomic-scale elements, the fully atomistic description is recovered. By further including adaptive remeshing of the finite element mesh, the QC method can follow the deformation as it evolves. However, the QC method also does not allow for the continuum description of a dislocation, and therefore every dislocation in the QC model requires a full complement of atomistic degrees of freedom around its core and slip plane. This means that only a few dislocations can be present in a QC simulation before the computational cost becomes comparable to that of the fully atomistic description. In all of the methods to date, the "interesting" (i.e. non-linear) physics remains confined to regions that are resolved in full atomistic detail. These methods do provide a mechanism for avoiding finite-size boundary effects that can plague standard atomistic simulations and do minimize the number of atoms that need to be treated explicitly, but do not overcome other limitations of atomistic-scale simulations arising due to significant dislocation motion.

To extend the state-of-the-art in multiscale modeling, we describe here a new hybrid scheme coined the "coupled atomistic and discrete dislocation" (CADD) model. The CADD approach is similar to the FEAt and CLS approaches in that it begins from a separation of the physical problem into spatial regions that are modeled either by a fully atomistic description or by continuum finite elements. CADD extends these methods, however, by allowing for the presence and movement of continuum discrete dislocations in the continuum regime that interact with each other and with the atoms in the atomistic region via their elastic fields.

The philosophy behind the CADD method is that atomistic resolution is required in some regions of a material, but away from those regions the deformation is well-described by elasticity plus the plasticity due to the motion of well-defined continuum dislocations whose interactions can be described by elastic continuum fields. The dislocation behavior and assumptions made in the continuum region are essentially identical to those of the DD model, and CADD can incorporate any of the "constitutive" rules used in existing DD techniques. There are a wide variety of problems that satisfy the assumptions necessary for the CADD formulation, including nano-indentation, fracture, grain boundary sliding, slip transmission across grain boundaries and void nucleation and growth in crystals.

The current implementation of CADD is for a two-dimensional (2D) problem. Only dislocations with a line direction perpendicular to the x–y plane of the model are permissible, but their character can be edge, screw or mixed. This is accommodated by employing periodic boundary conditions along the z-axis in the atomistic region and by

allowing 3 degrees of freedom (displacements u_x, u_y and u_z) in the two-dimensional (x–y) continuum region. The 2D implementation permits dislocations to automatically move across the interface between the atomistic and the continuum region, taking correct account of the attendent kinematics of the deformation as the dislocation is "converted" from a defect in atomic arrangement to a displacement field in an elastic continuum, or vice-versa. Extension to three dimensions is not a trivial matter, but is a subject of current research. As well, the CADD method presented here is for static equilibrium solutions, so there are no temperature or dynamic effects, although such extensions are quite feasible.

The remainder of this paper is organized as follows. In Section 2, the details of the CADD coupling between the atomistic and continuum regions are provided, while the details of automatically detecting and passing dislocations between the two domains are provided in Section 3. We present two tests to validate the method in Section 4: First, we systematically shrink the size of the atomistic region around a crack tip, and show that the CADD method accurately predicts the critical stress intensity factors for the crack even when the atomistic region is very small. Second, indentation by a square punch is compared to a fully atomistic simulation of the same problem. In Section 5, we provide a brief overview of two more applications that will be studied in detail in future publications: nano-indentation by a spherical indenter and atomic scale void growth under uniaxial tension. We then conclude the paper with a summary to highlight the main conclusions.

Note that the present CADD method is completely distinct from another coupling technique recently developed by the same authors (Shilkrot et al., 2002a), which is more accurate in principle but more unwieldy in practice; we thus advocate future use of the current method. A preliminary model similar to CADD was presented by Wei Yang et al. (1994), but it suffered from a cumbersome dislocation passing technique and was apparently not extended to general problems. A short publication describing CADD has appeared previously (Shilkrot et al., 2002b), but we emphasize that since the time of that publication, we have significantly modified the nature of the atomistic/continuum coupling at the interface. Our original coupling method was clearly shown in Curtin and Miller (2003) to have some spurious effects. The new coupling used here, which is essentially that of Kohlhoff et al. (1991), was shown in Curtin and Miller (2003) to be significantly more accurate.

2. Model formulation

The CADD method consists of four essential components: the atomistic model, the discrete dislocation framework, the coupling between these regions, and the method for detecting and passing dislocations between the two regions. The first two components, the atomistics and DD framework, are not new to this work, and are simply taken from the well-developed methods found in the literature. The atomistic framework we adopt is the embedded atom method (EAM) of Daw and Baskes (1984), although the method can, in principle, be extended to more sophisticated atomistic approaches. The DD formulation we adopt is essentially that of van der Giessen and Needleman

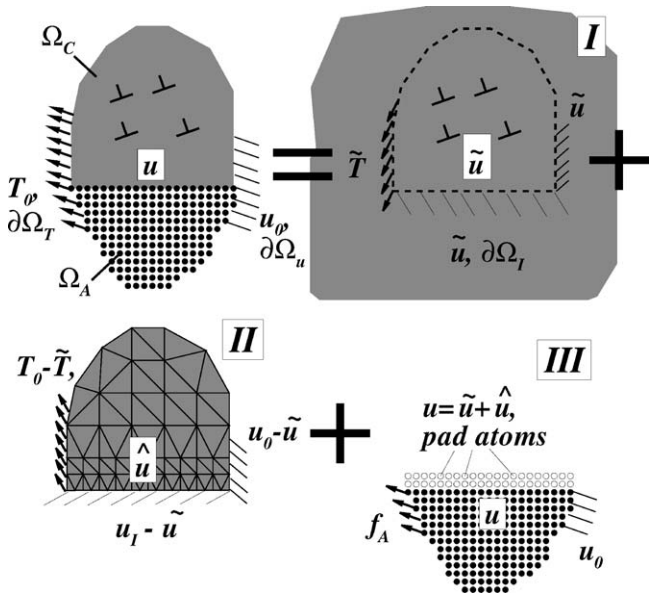

Fig. 1. Schematic illustration of the solution procedure for coupled atomistics and discrete dislocation plasticity. The continuum is coupled to the atomistic region by the displacements of the atoms on the interface, $\boldsymbol{u}_I$, while the atoms are coupled to the continuum by the pad atoms whose displacements are dictated by the continuum fields.

(1995). The important new contributions in this work are the details of coupling the two regions and the automatic detecting and passing dislocations from the atomistic region to the continuum, and vice versa. Both are described in detail in the following sections.

2.1. Atomistic/continuum coupling

The general boundary value problem we wish to solve is shown schematically in the top left of Fig. 1. A body Ω is subjected to prescribed traction $\boldsymbol{T} = \boldsymbol{T}_0$ on $\partial\Omega_T$ and displacements $\boldsymbol{u} = \boldsymbol{u}_0$ on $\partial\Omega_u$. The body is imagined to be divided into an atomistic region Ω_A and a continuum region Ω_C, joined at an interface $\partial\Omega_I$ defined by a line of atoms (shown as the topmost row of atoms in Fig. 1(a)). This interface need not be straight. Tractions on $\partial\Omega_A$ are inherently discrete, so it is more natural to treat the loads applied to $\partial\Omega_A$ as lumped forces $\boldsymbol{f}_A$ on individual atoms. The body contains N continuum dislocations, for which the ith dislocation has Burgers vector $\boldsymbol{b}^i$ and position $\boldsymbol{d}^i$. Each material point in the continuum and each atom in the atomistic region has a reference position $\boldsymbol{X}$ in the undeformed, defect free body, and experiences a displacement $\boldsymbol{u}$, which brings it to the deformed configuration $\boldsymbol{x} = \boldsymbol{X} + \boldsymbol{u}$. We wish to solve this boundary value problem for the equilibrium stress $\boldsymbol{\sigma}$, strain $\boldsymbol{\varepsilon}$, displacement fields $\boldsymbol{u}$, and discrete dislocation positions $\boldsymbol{d}^i$ in the continuum, and simultaneously for

the equilibrium positions of the atoms, as a function of the imposed boundary conditions. The method naturally allows for any number of atomistic and continuum regions, singly or multiply connected, however the development presented in the remainder of this paper is, for clarity and simplicity, restricted to a single atomistic region adjoining a single continuum region.

It is convenient to distinguish between quantities that are associated with the interface, points in the continuum, and atoms in the atomistic region, and in what follows we will use the subscripts I, C and A, respectively. In the atomistic region, any number of atomic defects such as dislocations, grain boundaries, vacancies, voids, or amorphous regions may be present. The degrees of freedom in this region are the atoms themselves, with positions $\boldsymbol{r}_A$ and $\boldsymbol{r}_I$. The only assumption about these atomistic regions is that near the atomistic/continuum interface their behavior approaches the linear elastic response used to describe the continuum. The only non-linear behavior allowed to "pass" across the atomistic/continuum interface is the core of a dislocation, as will be discussed in Section 3. In the continuum region, the only permitted defects are the continuum dislocations. In a finite element representation of the continuum elastic behavior, the degrees of freedom in the continuum are then the finite element nodal displacements $\boldsymbol{U}_C$ and $\boldsymbol{U}_I$ and the discrete dislocation positions $\boldsymbol{d}^i$. Note that the discretization of the continuum region matches the atomistic lattice at the interface: the interface atoms $\boldsymbol{r}_I$ are also interface nodes with displacements $\boldsymbol{U}_I$ for the continuum.

The precise coupling at the interface $\partial\Omega_I$ between an atomistic region and a continuum region requires careful attention. The atomistic region is inherently non-local, due to the extended beyond-near-neighbor range of realistic interatomic potentials, and the continuum region is local, since stresses at a point in the continuum are completely determined by the deformation *at that point*. Abruptly terminating atomistic material along an atomic plane to create separated atomistic and continuum regions (as illustrated schematically in Fig. 1), or abruptly beginning a finite element description of the material, introduces a spurious surface energy and non-physical interface reconstructions, as atoms within the range of the interatomic interactions of the interface will not have proper atomic coordination. Numerous approaches have been used to avoid the problems that ensue, including the addition of corrective so-called "ghost forces" (Shenoy et al., 1998), a transition region of non-local continuum finite elements (Kohlhoff et al., 1991), and force or energy averaging techniques that mitigate the abrupt transition (Rudd and Broughton, 2000). Two of the authors have written a recent review detailing the various approaches to this issue (Curtin and Miller, 2003), quantifying the degree and nature of the ghost forces for each of these coupling schemes. Here, we use the most accurate coupling method devised to date, which is essentially that of the FEAt method (Kohlhoff et al., 1991) without the use of non-local finite elements. We note that the main distinguishing feature of the CADD method (i.e. the multiscale treatment of dislocations) is independent of the coupling scheme, such that CADD can use any of the techniques previously developed.

To ensure that real atoms at and near the interface are properly coordinated, we introduce a pad of atoms that overlaps with the continuum region. This pad region is shown in Fig. 2(a), and the positions of the pad atoms are denoted by $\boldsymbol{r}_P$. The minimum thickness of the pad must exceed the range of interatomic interactions r_{cut} in

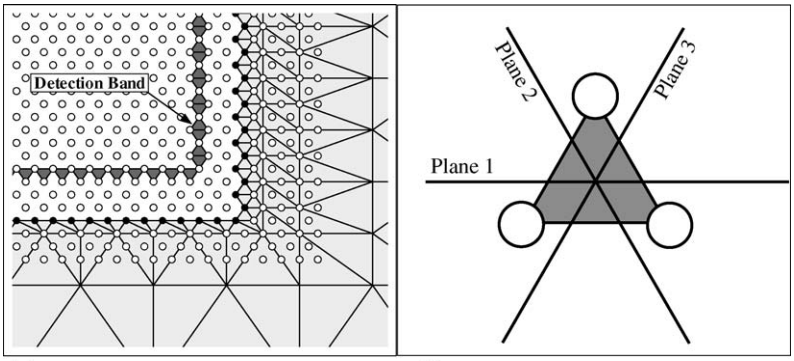

Fig. 2. (a) Close-up of the atomistic/continuum interface. Continuum elements are light grey. Dark grey elements are used in dislocation detection but do not contribute to the energy. The actual interface between the two regions is made up of the atom/nodes shown by filled circles, while unfilled circles that lie inside the continuum region are used as a "pad" of atoms to couple the atoms to the continuum region. (b) A close-up of one detection element, indicating the three slip planes on which it lies.

the material. The pad thickness must also be such that real atoms continue to see a full complement of surrounding atoms after dislocations have passed between the atomistic and continuum regions, which generates slip steps at the interface. The positions $\boldsymbol{r}_P$ of the pad atoms are determined completely by the deformation of the continuum region in which the pad atoms reside. That is, given the nodal displacements as obtained from the continuum solution (see below), the pad atom positions are given by interpolating the nodal displacements to the crystal lattice sites of the pad atom reference positions inside each finite element. From the viewpoint of the real atoms and interface atoms (degrees of freedom r_A and r_I), the pad atom positions are instantaneously fixed. This approximation makes use of our underlying assumption that the displacement field $\boldsymbol{u}$ in the continuum region is a good approximation to the real field of atomic displacements.

The total free energy for the atomistic domain includes interactions with the pad atoms. Denoting as E_i the energy of the ith atom as determined from the EAM function, the total atomistic free energy functional is given by

$$E^{\mathrm{a}} = \sum_{i\in(A,I,P)} E_i(\boldsymbol{r}_A, \boldsymbol{r}_I, \boldsymbol{r}_P) - \boldsymbol{f}_A \cdot \boldsymbol{u}_A \tag{1}$$

where $\boldsymbol{u}_A$ are the atom displacements. The sum over atoms includes the pad atoms, although these are not degrees of freedom. Partial derivatives of E^{a} with respect to positions $\boldsymbol{r}_A$ and $\boldsymbol{r}_I$ then yield full atomistic forces on the atoms,

$$\boldsymbol{f} = -\left(\frac{\partial E^{\mathrm{a}}}{\partial \boldsymbol{r}_A}\right). \tag{2}$$

The force computed for atoms at or in the vicinity of the interface is a real physical force produced by the local atomic environment. Partial derivatives of E^{a} with respect to pad atoms P would generally include non-physical surface effects, but these derivatives

are simply not taken because they are not needed; the pad atom positions are completed dictated by the displacements in the continuum elements.

The total free energy functional for the continuum domain is calculated as discussed below, but in general is expressed as a sum over the energies E_μ of the finite elements μ plus boundary work terms as

$$E^{\mathrm{c}} = \sum_{\mu} E_\mu(\boldsymbol{U}_I, \boldsymbol{U}_C, \boldsymbol{d}^i) - \int_{\partial\Omega_T} \boldsymbol{T}_0 \boldsymbol{u} \, \mathrm{d}A \tag{3}$$

which depends on the displacements $\boldsymbol{U}_I$ of the nodes on the interface, the displacements of the nodes $\boldsymbol{U}_C$ in the discretized continuum (see below), and the positions $\boldsymbol{d}^i$ of the discrete dislocations. Relevant to the atomistic/continuum coupling is that the displacements of the interface nodes are not degrees of freedom but rather are determined from the current atom positions through $\boldsymbol{U}_I = \boldsymbol{r}_I - \boldsymbol{R}_I$, where $\boldsymbol{R}_I$ is the initial, reference atom position. In other words, the interface atoms are moved as atoms and from the point of view of the continuum they are fixed nodes with prescribed displacements $\boldsymbol{U}_I$.

In this formulation, the pad and interface atoms serve several important purposes. First, the pad atoms ensure that real atoms in the vicinity of the interface are properly coordinated. Second, the pad atoms inform the atomistic region about the deformation in the continuum region and, similarly, the interface atoms inform the continuum about the deformation in the atomistic region. Because the atoms are non-local, a finite thickness pad is required to transmit the continuum deformation to the atoms. In contrast, because the finite element continuum is local, only a set of interfacial atoms are required to transmit the atomistic deformation to the continuum.

Note that the energy E^{a} includes the elastic energy of the pad atoms whose energy is already implicitly contained in the continuum energy E^{c}. A true total energy for the system cannot be unambiguously defined without spurious interfacial forces or displacements (Curtin and Miller, 2003). This is the key tradeoff between the coupling scheme we use here and schemes like those of QC and CLS: our coupling scheme does not suffer from spurious forces at the interface, but the CLS and QC methods both have a well-defined energy functional. Without a total energy from which all forces can be derived, we cannot use the standard, computationally efficient, conjugate gradient method to drive the entire system toward equilibrium. When extended to dynamic approaches, a proper total energy is a convenient tool to monitor the stability of the evolving dynamic system and to formally ensure that the model has time-reversal symmetry, but a well-defined energy is not a requirement. For the static equilibrium problems addressed here, equilibrium will be found using the forces only, however, as discussed in Section 2.3.

2.2. Continuum region with discrete dislocations

We now specify the energy functional E^{c} for the continuum region containing discrete dislocations. The boundary value problem for the continuum region, at any instant for which the dislocations are at positions $\boldsymbol{d}^i$, is defined by the boundary conditions on $\partial\Omega_C$ and the fixed displacements $\boldsymbol{U}_I$ along $\partial\Omega_I$ that are obtained from the interface atom positions $\boldsymbol{r}_I$, which enforces compatibility between the atomistic and continuum

regions. Thus, for a given set of atomic displacements $\boldsymbol{U}_I$, the continuum problem is a well-posed, fully specified, discrete dislocation boundary value problem. It is solved using an approach very similar to that of the standard DD methodology described in van der Giessen and Needleman (1995), as follows.

The continuum elastic problem is itself divided into two complementary problems I and II, as shown in Fig. 1. Problem I corresponds to the discrete dislocations residing in an infinite homogeneous elastic material. The solution for the total stress $\tilde{\boldsymbol{\sigma}}$, strain $\tilde{\boldsymbol{\varepsilon}}$ and displacements $\tilde{\boldsymbol{u}}$ in Problem I is then simply the superposition of the known elastic fields due to all the dislocations at positions $\boldsymbol{d}^i$ in an infinite elastic continuum, given by

$$\tilde{\boldsymbol{\sigma}} = \sum_i^N \tilde{\boldsymbol{\sigma}}^i, \quad \tilde{\boldsymbol{\varepsilon}} = \sum_i^N \tilde{\boldsymbol{\varepsilon}}^i, \quad \tilde{\boldsymbol{u}} = \sum_i^N \tilde{\boldsymbol{u}}^i, \tag{4}$$

where $\tilde{\boldsymbol{\sigma}}^i$, $\tilde{\boldsymbol{\varepsilon}}^i$ and $\tilde{\boldsymbol{u}}^i$ are the linear elastic solutions for the fields of the ith dislocation in the infinite material. The fields of Problem I do not satisfy the overall boundary conditions. Rather, the superposition leads to tractions $\tilde{\boldsymbol{T}}$ along the surfaces $\partial\Omega_T$ and some displacements $\boldsymbol{u} = \tilde{\boldsymbol{u}}$ along $\partial\Omega_u$ and $\partial\Omega_I$ that differ from the desired $\boldsymbol{T}_0$, $\boldsymbol{u}_I$ and $\boldsymbol{u}_0$. Problem II is designed as a "corrective" boundary value problem whose fields, when superposed with those of Problem I, lead to fields that satisfy the true boundary conditions. Problem II is thus a boundary value problem for a linear elastic body, containing no dislocations, to which the corrective tractions $\hat{\boldsymbol{T}} = \boldsymbol{T}_0 - \tilde{\boldsymbol{T}}$ (on $\partial\Omega_T$) and corrective displacements $\hat{\boldsymbol{u}} = \boldsymbol{u}_0 - \tilde{\boldsymbol{u}}$ (on $\partial\Omega_u$) and $\hat{\boldsymbol{u}} = \boldsymbol{u}_I - \tilde{\boldsymbol{u}}$ (on $\partial\Omega_I$) are applied as boundary conditions. Because all the discontinuities and singularities associated with the dislocations are contained in the $\tilde{}$ fields of Problem I, the fields of Problem II are smooth and, therefore, can be solved accurately using the finite element method for general geometries and loading configurations. The displacements, stresses, and strains of Problem II are denoted by $\hat{}$. The total fields in the continuum region are then

$$\boldsymbol{u} = \tilde{\boldsymbol{u}} + \hat{\boldsymbol{u}}, \quad \boldsymbol{\sigma} = \tilde{\boldsymbol{\sigma}} + \hat{\boldsymbol{\sigma}}, \quad \boldsymbol{\varepsilon} = \tilde{\boldsymbol{\varepsilon}} + \hat{\boldsymbol{\varepsilon}}, \tag{5}$$

which satisfy the boundary conditions imposed on the continuum region by construction and equilibrium by linear elastic superposition.

In our implementation, we use the fully anisotropic, linear elastic constitutive relation for Problem II, so that the continuum elastic constants matched those of the crystalline atomistic region. However, for the $\tilde{}$ fields of Problem I describing the discrete dislocations, we use the analytic fields from *isotropic* elasticity with the Voigt-averaged elastic constants (Hirth and Lothe, 1992). Thus, the constitutive relations in the continuum region are

$$\tilde{\sigma}_{ij} = 2\mu\tilde{\varepsilon}_{ij} + \lambda\tilde{\varepsilon}_{kk}\delta_{ij} \tag{6}$$

$$\hat{\sigma}_{ij} = c_{ijkl}\hat{\varepsilon}_{ij}, \tag{7}$$

where μ and λ are the Voigt-average elastic constants found from the fully anisotropic modulus tensor c_{ijkl}. The fully anisotropic solution is thus obtained in the special case when no discrete dislocations are present, but small errors are introduced through the $\tilde{}$ fields when discrete dislocations exist.

From the above decomposition, the free energy functional E^{c} for the continuum region is

$$E^{\mathrm{c}} = \frac{1}{2}\int_{\Omega_C} (\hat{\boldsymbol{\sigma}} + \tilde{\boldsymbol{\sigma}}) : (\hat{\boldsymbol{\varepsilon}} + \tilde{\boldsymbol{\varepsilon}})\,\mathrm{d}V - \int_{\partial\Omega_T} \boldsymbol{T}_0(\tilde{\boldsymbol{u}} + \hat{\boldsymbol{u}})\,\mathrm{d}A. \tag{8}$$

After discretization of the $\hat{}$ in a finite element implementation, introduction of the Airy Stress function χ for the individual dislocation $\tilde{}$ fields, application of the principle of virtual work, and other manipulations, as detailed in the appendix, the energy functional can be written in the form

$$\begin{aligned} E^{\mathrm{c}} = {} & \frac{1}{2}(\hat{\boldsymbol{u}}_C \cdot \boldsymbol{C}_{CC} \cdot \hat{\boldsymbol{u}}_C + \hat{\boldsymbol{u}}_I \cdot \boldsymbol{C}_{II} \cdot \hat{\boldsymbol{u}}_I) + \hat{\boldsymbol{u}}_C \cdot \boldsymbol{C}_{CI} \cdot \hat{\boldsymbol{u}}_I \\ & + \frac{1}{2}\sum_{l\neq m}\left(\frac{\partial \chi^l}{\partial y} b_x^m - \frac{\partial \chi^l}{\partial x} b_y^m\right) - \frac{1}{2}\int_{\partial\Omega_C+\partial\Omega_I}\left(\frac{\partial \chi}{\partial y}\nabla \tilde{u}_y - \frac{\partial \chi}{\partial x}\nabla \tilde{u}_x\right)\mathrm{d}\boldsymbol{A} \\ & - \boldsymbol{t}_0 \cdot (\tilde{\boldsymbol{u}}_C + \hat{\boldsymbol{u}}_C) + \tilde{\boldsymbol{t}}_C \cdot \hat{\boldsymbol{u}}_C, \end{aligned} \tag{9}$$

where $\boldsymbol{C}$ are the stiffness matrices resulting from the finite element discretization of the continuum. The equilibrium $\hat{}$ fields are then obtained by minimizing Eq. (9) with respect to the unconstrained $\hat{\boldsymbol{u}}_C$ degrees of freedom, i.e.

$$\frac{\partial E^{\mathrm{c}}}{\partial \hat{\boldsymbol{u}}_C} = 0 = \boldsymbol{C}_{CC}\hat{\boldsymbol{u}}_C + \boldsymbol{C}_{CI}\hat{\boldsymbol{u}}_I - \hat{\boldsymbol{t}}_C. \tag{10}$$

The solutions for the unconstrained $\hat{\boldsymbol{u}}_C$ can be obtained explicitly in terms of the constrained $\hat{\boldsymbol{u}}_C$ on the boundary $\partial\Omega_C$ and the interface degrees of freedom $\hat{\boldsymbol{u}}_I$ as

$$\hat{\boldsymbol{u}}_C = \boldsymbol{C}_{CC}^{-1}(\hat{\boldsymbol{t}}_C - \boldsymbol{C}_{CI}\hat{\boldsymbol{u}}_I). \tag{11}$$

Note that the solution for the $\hat{\boldsymbol{u}}_C$ involves the inverse of the stiffness matrix $\boldsymbol{C}_{CC}$. Although this is a large matrix, the inverse must only be calculated once at the start of the simulation. Subsequently, $\boldsymbol{C}_{CC}^{-1}$ only appears in matrix multiplications. In essence, elimination of the $\hat{\boldsymbol{u}}_C$ degrees of freedom corresponds to the well-known technique of substructuring in finite elements or equivalently to the calculation of the numerical Green's function for the elastic continuum region. Substituting the solution for the $\hat{\boldsymbol{u}}_C$ back into Eq. (9) leads to a reduced energy functional for the continuum system in which the only remaining degrees of freedom are the discrete dislocation positions $\boldsymbol{d}^i$. This continuum energy functional is used to obtain forces on the discrete dislocations as described next.

2.3. Equilibrium configurations

The CADD formulation, as described above, includes two free energy functionals which depend on the degrees of freedom, atom and discrete dislocation positions, that must be brought to equilibrium after each increment of external loading. Rather than minimizing the total energy, we search for the point in configuration space where the

forces applied to the degrees of freedom are zero. These forces are obtained from the derivatives of the atomistic and continuum energy functionals. The force on the ith dislocation is the Peach–Koehler (P–K) force $\boldsymbol{p}^i$ given by the negative of the derivative of the elastic energy of the continuum region E^{c} with respect to the position dislocation $\boldsymbol{d}^i$,

$$\boldsymbol{p}^i = -\frac{\partial E_C}{\partial \boldsymbol{d}^i}. \tag{12}$$

Constraining motion of the discrete dislocations to the slip plane (i.e., no dislocation climb or cross-slip), Eq. (12) can be replaced by

$$p^i = -\frac{\partial E^{\mathrm{c}}}{\partial s^i} = (\boldsymbol{m}^i)^{\mathrm{T}} \left(\hat{\boldsymbol{\sigma}} + \sum_{j \neq i}^{N} \tilde{\boldsymbol{\sigma}}^j \right) \boldsymbol{b}^i, \tag{13}$$

where s^i is the position of a dislocation along its slip plane, $\boldsymbol{m}^i$ is the slip plane normal, and $\boldsymbol{b}^i$ is the Burgers vector. This expression for the P–K force along the slip plane was derived in van der Giessen and Needleman (1995), and demonstrates that the P–K force can be obtained directly from the stress fields calculated in Problems I and II. The finite element solution to the stress field $\hat{\boldsymbol{\sigma}}$, obtained at the Gauss points of the element, is not smooth across element interfaces, however. Hence, the approximate stress fields must be interpolated and smoothed to minimize artifacts. Alternatively, we have found it computationally effective to directly calculate the P–K forces numerically during our solution procedure. This does not lead to an onerous computational overhead for moderate numbers of dislocations since each dislocation has only one degree of freedom in 2D.

With the forces obtained from Eqs. (2) and (13), we have modified the standard conjugate gradient method (Press et al., 1992) to search for the point of zero forces on all degrees of freedom. At the beginning of each iteration we pick the direction of descent using the standard conjugate gradient procedure for which the value for the energy is not required but only its derivatives (forces). Along this direction, we then find a point where the force along this direction is zero. At such a point, the vector of forces is perpendicular to the direction of descent, which is exactly the condition required in the conjugate gradient method in order to chose the direction for the next iteration.

In the search for the equilibrium configuration, atomic coordinates and dislocation positions are updated simultaneously. Given updated interface atom and discrete dislocation positions we solve for the continuum displacements and update the positions of atoms in the pad. The P–K forces p^i acting on dislocations and the forces $\boldsymbol{f}_A$ acting on the atoms are computed and supplied to the modified conjugate gradient algorithm, which outputs atomic and discrete dislocation positions that have been updated along the search direction.

As we shall demonstrate in Section 4, this force-based coupling allows the interface to be brought remarkably close to the region of non-linear atomistic behaviour with almost no ill-effect on the results obtained from the simulation.

3. Dislocation detection and passing

3.1. Issues in the passing of dislocations

Dislocations nucleated in the atomistic region, or generated from sources placed inside the continuum region, may experience driving forces to move from the atomistic region into the continuum region, or vice-versa. Because of the seamless nature of the atomistic/continuum interface for elastic deformations, the dislocations do not sense the existence of the interface when the dislocation is a modest distance away. As an atomistic dislocation, i.e. a dislocation with a real atomistic core structure, approaches the interface, however, spurious forces are generated: the elastic continuum is not able to properly accomodate the shear deformation associated with the burgers vector of the dislocation. It resists this shear by a fully elastic response, whereas in the true atomistic case the non-linear response leads to softening under this shear, which permits continued glide of the dislocation. Thus, atomistic dislocations approaching the interface must be detected and artificially moved across the interface. In this process, the atomistic core structure must be eliminated from the atomistic region and a continuum discrete dislocation must be introduced appropriately into the continuum problem.

It is instructive to clearly demonstrate the spurious effects of the dislocation/interface interaction by means of an example, which will also provide a basis for understanding the details of the detecting and passing algorithm discussed below. Therefore, consider the problem of an atomic scale void in a single crystal of fcc Ni containing no other defects, modeled using the methodology described in the previous section. The mesh for the problem is shown in Fig. 3, with a close-up of the atomistic region shown in the inset, with a mesh between the atoms to aid visualization of the atomistic deformations. The model is loaded in uniaxial tension by incrementally superimposing

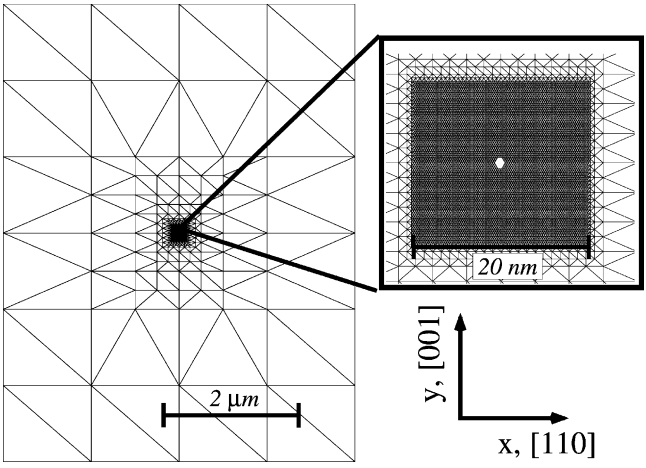

Fig. 3. Model used to study growth of an atomic-scale void due to plastic deformation. Material is fcc Ni, oriented as shown.

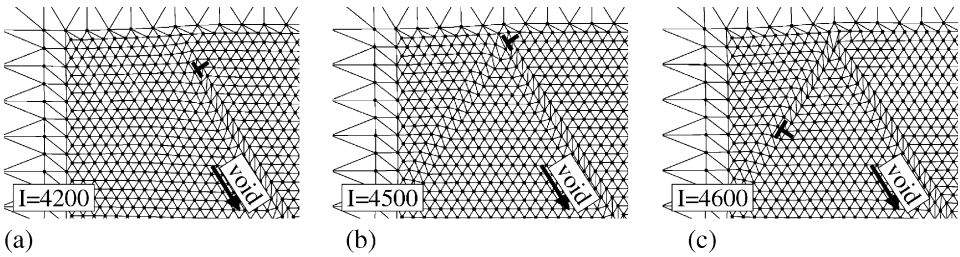

Fig. 4. A series of deformation steps during energy minimization illustrating the non-physical reflection of a dislocation that is not allowed to pass across the atomistic/continuum interface. The mesh is drawn between the atoms in the atomistic region for visualization purposes—the deformed elements clearly highlight the slip plane in the wake of the dislocation.

a uniform strain in the y-direction, and fixing the y-component of displacement on the top and bottom boundary.

Monitoring the atom displacements *during* conjugate gradient minimization, at a macroscopic strain of $\varepsilon = 0.086$, we observe a dislocation nucleated from one corner of the void which moves toward the atomistic/continuum interface. The sequence of the deformation is shown in Fig. 4 with frames labelled according to the number of conjugate gradient iterations performed (I) and the dislocation core indicated by the inverted "T". Slip between crystal planes can be seen in the shear deformation of the mesh elements lying along the glide path between the core and the void. As the dislocation approaches the interface, the inability of the continuum region to accomodate the displacement discontinuity of the Burgers vector leads to non-physical reflection of the dislocation off of the interface as shown in configuration Fig. 4(c), with a residual interface "dislocation" left behind. In a fully atomistic simulation, the dislocation would continue gliding outward along the original glide plane. In CADD, an algorithm to detect the dislocation as it approaches the interface and then pass it to the continuum region as a continuum discrete dislocation is needed to accurately represent the true deformation behavior.

3.2. Detecting dislocations

Dislocations in the atomistic region must be detected and passed *before* reaching the interface. As a first step, we define a "detection band" of elements in the atomistic region in a thin strip some short distance from the interface, as shown by the darkly shaded elements in Fig. 2(a). A single element from this band is shown in isolation in Fig. 2(b). Note that these elements are used for monitoring the kinematics of the deformation and play no role in calculating energies or forces in the atomistic region. We must then define a kinematic criterion that can unambiguously detect the slip in these elements and devise an algorithm to determine if that slip is associated with a dislocation. Other authors (see for example, Zimmerman et al., 2001) have developed definitions of atomic level slip that are useful for visualization of slip processes, but they cannot easily be adapted to our problem where the identity of each individual

dislocation must be made exactly. First, during the course of a simulation, many dislocations may pass through a certain region or single detection band element and it is necessary to separate out the relevant slip due to each dislocation. Second, the displacements of the three atoms that define the nodes of a detection element will include not only slip but also elastic deformation, rigid body translation, and rotation which must be "filtered out" in some way. With these stringent requirements, we find it necessary to make use of the following three key components: (i) all deformation is referred back to the reference configuration of a perfect crystal, i.e. a Lagrangian analysis of deformation is used, (ii) the defined slip measure must be invariant under rigid body rotation and translation of the lattice, i.e. a finite deformation analysis is used, and (iii) only deformation due to new slip is monitored by keeping track of all past slip activity. The first two requirements motivate the use of the local deformation gradient $\boldsymbol{F}$ and the extraction of the associated Lagrangian plastic (slip) strain tensor $\boldsymbol{E}^{\mathrm{p}}$ for each element. We thus proceed as follows.

Each atom has an undeformed position $\boldsymbol{X}$ and a deformed position $\boldsymbol{x} = \boldsymbol{X} + \boldsymbol{u}$. The displacements due to all previously passed dislocations must first be subtracting from the total displacements in the detection band before the elemental strains are computed. Then, the strain due only to new dislocations (plus a smaller elastic contribution) remains. We know all previously-passed dislocations and their positions in the continuum region. Because dislocations are confined to move in their slip plane in the continuum region (i.e. no cross slip can occur), the $\tilde{\boldsymbol{u}}$-field for each continuum dislocation includes a branchcut corresponding to the slip along the atomic planes in the atomic region. Subtracting the $\tilde{\boldsymbol{u}}$ displacements due to the continuum dislocations, we have the relevant residual displacement $\hat{\boldsymbol{x}} = \boldsymbol{X} + \hat{\boldsymbol{u}}$ where $\hat{\boldsymbol{u}} = \boldsymbol{u} - \tilde{\boldsymbol{u}}$. The deformation gradient $\boldsymbol{F}$ used to identify new slip is defined as

$$\boldsymbol{F} = \frac{\partial \hat{\boldsymbol{x}}}{\partial \boldsymbol{X}}. \tag{14}$$

Formally, we can decompose the deformation gradient into elastic and plastic parts and write

$$\boldsymbol{F} = \boldsymbol{F}^{\mathrm{e}}\boldsymbol{F}^{\mathrm{p}}. \tag{15}$$

An ideal slip deformation ($\boldsymbol{F}^{\mathrm{e}} = \boldsymbol{I}$) is depicted in Fig. 5. In the shaded element, nodes 1 and 2 have undergone rigid translation and rotation, while node 3 has moved by one Burgers vector along the slip plane. Since there is no material inside the element, uniform deformation can be assumed and hence the plastic deformation gradient can be decomposed as

$$\boldsymbol{F}^{\mathrm{p}} = \boldsymbol{R}\boldsymbol{U}^{\mathrm{p}}, \tag{16}$$

where $\boldsymbol{R}$ is a lattice rotation and $\boldsymbol{U}^{\mathrm{p}}$ is given by

$$\boldsymbol{U}^{\mathrm{p}} = \boldsymbol{I} + \frac{\boldsymbol{b} \otimes \boldsymbol{m}}{d}, \tag{17}$$

where $\boldsymbol{b}$ is the Burgers vector, $\boldsymbol{m}$ is the slip plane normal, d is the interplanar distance shown in Fig. 5 and $\otimes$ implies the tensor product. The finite Lagrangian strain of a detection band element is

$$\boldsymbol{E} = \tfrac{1}{2}[\boldsymbol{F}^{\mathrm{T}}\boldsymbol{F} - \boldsymbol{I}], \tag{18}$$

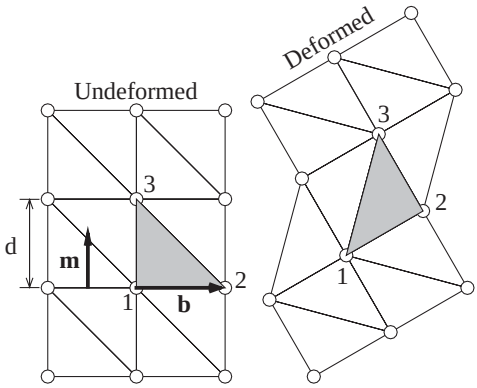

Fig. 5. Idealized deformation involving perfect slip and rigid body translation and rotation of the lattice.

where $\boldsymbol{I}$ is the identity matrix. Using the decomposed $\boldsymbol{F}$, we can then define the plastic slip strain tensor as

$$\boldsymbol{E}^{\mathrm{p}} = \frac{1}{2}[(\boldsymbol{F}^{\mathrm{p}})^{\mathrm{T}}\boldsymbol{F}^{\mathrm{p}} - \boldsymbol{I}] = \frac{(\boldsymbol{b}\otimes\boldsymbol{m})_{\mathrm{sym}}}{d} + \frac{(\boldsymbol{m}\otimes\boldsymbol{b})(\boldsymbol{b}\otimes\boldsymbol{m})}{2d^2}, \tag{19}$$

where $_{\mathrm{sym}}$ implies the symmetric part of the matrix.

We use $\boldsymbol{E}^{\mathrm{p}}$ to detect dislocations as follows. For a given crystal structure and orientation, we know the entire set of expected dislocations which may cross the atomistic/continuum interface. For example, in an FCC crystal there are 24 possible dislocations (4 slip planes, 3 Shockley partials on each, each of which can be positive or negative). Because $\boldsymbol{E}^{\mathrm{p}}$ is symmetric, it has only six unique components, and so we compute and store the six components of the plastic strain matrix $\boldsymbol{E}_i^{\mathrm{p}}$ for each of the i possible dislocations. For convenience, an additional "dislocation" is defined with Burgers vector $\boldsymbol{b} = \boldsymbol{0}$, corresponding to no slip in the element and $\boldsymbol{E}_i^{\mathrm{p}} = \boldsymbol{0}$. During a simulation, with each update of the atomic positions, we compute the actual strain in each detection band element, which is efficiently handled using isoparametric, constant strain triangular elements (see, for example, Zienkiewicz, 1991). These actual deformations include elastic deformations so that $\boldsymbol{F}^{\mathrm{e}} = \boldsymbol{I}$ is not generally satisfied. We thus identify the slip in each element as being due to that dislocation which minimizes the L_2 norm of the difference between the actual elemental strain and the dislocation plastic strain:

$$L_2 = \sqrt{(\boldsymbol{E} - \boldsymbol{E}_i^{\mathrm{p}}) : (\boldsymbol{E} - \boldsymbol{E}_i^{\mathrm{p}})}. \tag{20}$$

If the dislocation minimizing this norm has $\boldsymbol{b}=0$ then the element is undergoing only elastic deformation and no real dislocation is detected. Otherwise, it is assumed that the core of the detected dislocation is at the centroid of the element under consideration. With the spatial location, Burger's vector, and slip plane all identified by this detection algorithm, the identified dislocation can be passed to the continuum region, as discussed in the next subsection.

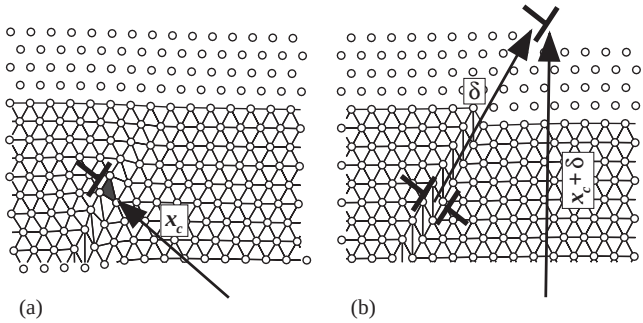

Fig. 6. The dislocation detected in the highlighted element in (a) is "passed" across the atomistic/continuum interface by superimposing the displacement field of the dipole shown in (b). A mesh is shown between atoms to help visualize the slip in the wake of the dislocation.

The main requirement for successful implementation of this detection algorithm is an *a priori* knowledge of the character of dislocations expected in a certain crystal. It can be used to detect partial dislocations as easily as full ones. Note however, that partial dislocations, once passed to the continuum as described in the next section, introduce a stacking fault and associated stacking fault energy. Inclusion of this stacking fault energy is possible within the DD framework used in CADD (see, for example, Shenoy et al., 2000), but we have not currently implemented this capability.

Empirical atomistic simulation of screw dislocations in bcc metals have shown that the cores are typically non-planar, and it is clear that our detection algorithm in its current form is dependent on dislocations being largely confined to their glide plane. However, *moving* bcc screw cores would still be detected using our algorithm. As shown in Vitek (1974), these cores collapses onto a single glide plane before moving under an applied stress.

3.3. Passing dislocations

Once a dislocation has been detected as outlined above, it is necessary to pass the dislocation into the continuum region as a continuum entity. "Passing" involves appropriately modifying the displacements of all atoms and nodes in the problem so that the core of the atomistic dislocation is eliminated while retaining the slip displacements. This is achieved by superimposing the continuum elastic displacements of a dislocation dipole onto those of the atoms and nodes, as illustrated in Fig. 6. The original dislocation in Fig. 6(a) has been identified (location, Burgers vector, slip plane) by the detection band and the superimposed dipole configuration is shown schematically in Fig. 6(b). This superposition annihilates the atomistic core at the original position $\boldsymbol{x}_c$ and replaces it with a continuum dislocation at the position $\boldsymbol{x}_c + \boldsymbol{\delta}$, which is in the continuum region and is added to the array of continuum dislocations.

The vector $\boldsymbol{\delta}$ is generally on the order of a few lattice spacings so that the effect of the superimposed dipole is short-ranged and confined to a few atoms surrounding the original core position. However, this "passing" approach assumes that the dislocation

reaching the detection band would, in a fully atomistic simulation, move across into the continuum region of space. Since the dislocation is detected during the minimization process, it is likely to have moved toward the interface, if not past it, in most cases. One measure of this likelihood (which we have not attempted) is to calculate the driving force on the dislocation in the detection band position. In practice, the assumption that the dislocation will move at least the distance $|\boldsymbol{\delta}|$ is consistent with the numerical nature of the calculation, as long as $|\boldsymbol{\delta}|$ is smaller than the typical increments of the discrete dislocation motions when finding their equilibrium positions in the continuum.

Since the original core was an atomistic dislocation and it has been "annihilated" using the displacements of a continuum elastic dislocation, there will be some residual displacements of the atoms within two or three lattice spacings of the original core, i.e. where elasticity fails. These non-physical residual displacements are removed by selecting a small number of atoms around the original core, within the cutoff radius of the interatomic potentials, and subjecting them to energy minimization while holding all other atoms fixed. All that remains of the dislocation in the atomistic region after this relaxation step is the slip plane of the dislocation that now resides in the continuum. Global force minimization is then restarted from this new configuration of atomic, nodal, and discrete dislocation positions.

There are two subtleties in the above passing of dislocations across the interface that should be noted. First, the displacement fields of an elastic continuum dislocation are unique only up to an arbitrary selection of the branchcut, across which there is a jump in the displacement field. At the atomic scale, the orientation of this branchcut is physically prescribed by the atomic planes over which slip has occurred, and care must be taken that the continuum dipole field matches the atomic displacements in this regard. Second, in multiply-connected continuum regions (i.e. an atomistic region embedded completely inside a continuum), the continuum displacement field of the dislocation will extend out the other side of the atomistic region and lead to incorrect results. This is easily remedied by including a discrete dislocation of opposite sign inside the atomistic region, which effectively negates the branch cut of the real defect in the continuum. This "image" defect is not actually present in the atomistic region, and only enters through the superposition of the dislocation fields leading up to the solution of the complementary problem depicted in Fig. 1. Physically, this image dislocation has a sensible interpretation, as one cannot generate dislocations inside a bulk material without also generating one of opposite sign. Inside the atomistic region, some atomic-scale process has driven the nucleation of the defect and left behind, for example, a surface step or grain boundary dislocation. The continuum need not know these atomistic details but does require that an image dislocation reside in the atomistic part of the problem.

The reverse passing procedure, from the continuum to the atomistic region, is considerably easier to achieve. If the P–K force on a dislocation is such that the minimization algorithm attempts to move the dislocation across the interface, this is easily detected geometrically. The dislocation is then inserted into the atomistic region, just inside the detection band, using the superposition of a dipole displacement field as outlined previously. The discrete dislocation is kept as an "image" dislocation so that its branch cut is correctly maintained in the continuum, and the minimization proceeds. Note that

the dislocation introduced into the atomistic region will initially not have the correct atomistic core structure, but this is quickly restored by subsequent relaxation.

The ability to pass dislocations back and forth between the two regions can occasionally lead to some oscillations of the defects across the interface during minimization. This has the effect of slowing down the convergence of some load increments, but has only rarely led to a failure to converge. In these instances, the equilibrium position of the dislocation is somewhere in or very near the interface. For our static formulation, we have found that these instances can be circumvented by slightly increasing or decreasing the size of the load increment. In a dynamic formulation, which is the goal of current work (see the discussion section), we expect these difficulties to largely disappear.

An important feature of the current technique for dislocation passing is that it ensures full compatibility and conservation of mass during the simulation. Early methods for dislocation passing (Shilkrot et al., 2002a; Wei Yang et al., 1994) require the removal or addition of atomic half-planes to achieve the dislocation passing. Such approaches violate conservation laws, and furthermore are somewhat cumbersome and difficult to apply in general situations.

4. Validation

4.1. Brittle crack growth

We first investigate the accuracy of the atomistic/continuum interface coupling without the intervening issue of dislocation nucleation and passing. This is accomplished by calculating the critical stress intensity factor for crack growth in a brittle system as a function of the size of the atomistic region. As the interface is moved close to the high stress gradient near a crack tip, it is expected that the interface coupling will cause some deviation in the onset of crack growth and/or crack closure. Here, we show that even down to an atomistic region containing only 45 real atoms (including the interface atoms) the critical stress intensity factors for crack extension (K_{Ic}^{+}) and crack closure (K_{Ic}^{-}) vary from those found using the large atomistic regions by only a few percent. A similar study was carried out by Kohlhoff et al. (1991) and later expanded by Gumbsch and Beltz (1995) for the FEAt model.

The material studied here is hexagonal Al oriented with the c-axis out-of-plane, so as to create an effectively 2D atomistic region. The Ercolessi–Adams Al EAM potential is used for the atomistic interactions in this structure. The elastic constants for this hexagonal Al show that the material is unstable in out-of-plane shear but here we only permit 2D in-plane deformations. The in-plane properties, as determined from a separate atomistic simulation, are an equilibrium lattice constant of $a_0 = 2.83$ Å, and in-plane elastic moduli $C_{11} = C_{22} = 0.9581$ eV/Å^3, $C_{12} = \lambda = 0.5747$ eV/Å^3 and $C_{66} = \mu = 0.1917$ eV/Å^3. These in-plane elastic constants are used to fix the elastic constants for the finite element problem.

The geometry of the sample studied is a square box of size approximately 1 μm × 1 μm with a crack extending from the center of the left edge into the center of the box.

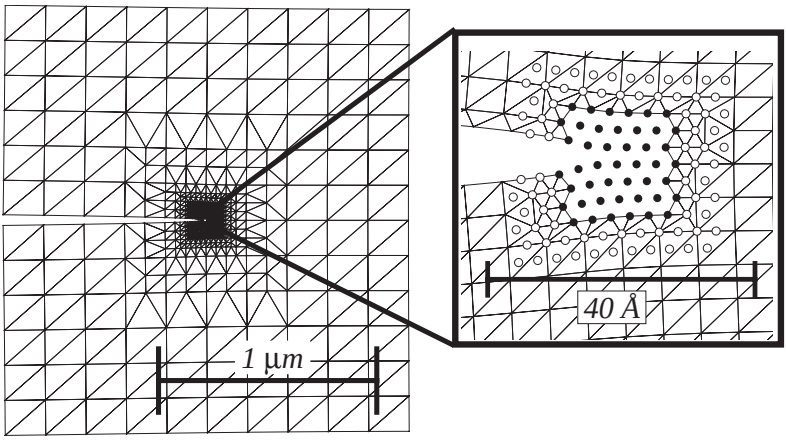

Fig. 7. Model used to study the effect of the size of the atomistic region on the computed critical stress intensity factor. Shown is the model with the smallest atomistic region containing only 45 atoms. Close-up of crack tip shows real atomistic region in black and surrounding pad atoms as white.

An atomistic region surrounds the crack tip, and the size of this atomistic region is varied systematically from approximately 100×100 Å down to approximately 21×8 Å. The entire computational problem and an enlarged picture of the smallest atomistic region and associated pad are shown in Fig. 7.

To drive the crack, displacements of all atoms and nodes are initialized at the positions dictated by the continuum solution for a semi-infinite crack under applied stress intensity K_I, with the crack tip position specified. The in-plane hexagonal Al is isotropic, and hence the isotropic displacement solution is accurate. The outer boundary is held fixed, while all interior atoms and nodes are allowed to relax. The crack faces in the continuum regime are traction-free while the atoms across the near-tip crack faces interact with the full potentials. Thus, the crack faces can close-up in the atomistic regime if the applied stress intensity is not sufficiently high.

Hexagonal Al exhibits lattice trapping under the quasistatic, zero temperature situation considered here. Thus, there is a range of applied stress intensity around the thermodynamic Griffith critical value K_{Ic} for which the crack tip remains at the position used in the applied boundary conditions. At an applied stress intensity K_{Ic}^{+} above the Griffith value, the crack grows forward. At an applied stress intensity K_{Ic}^{-} the crack recedes backward. The results for crack growth predicted using the CADD atomistic/continuum interface with various sizes of the atomistic region are shown in Fig. 8. In most cases, the applied stress intensity was increased or decreased from a stable value of 0.28 eV $\text{Å}^{-5/2}$ in increments of 0.002 eV $\times$ $\text{Å}^{-5/2}$ until the crack was observed to grow forward or recede. Fig. 8 shows both the last stable value of the stress intensity and the stress intensity at which the crack moved, for both growth and closing. Each pair of curves in the figure, in other words, represent upper and lower bounds on the exact value, which could be brought into better agreement by taking smaller increments than the 0.002 eV $\text{Å}^{-5/2}$ used here. As seen in Fig. 8, the

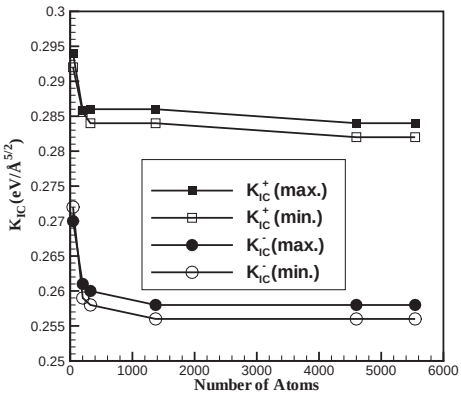

Fig. 8. Computed critical stress intensity factors for crack growth or recession as a function of the number of atoms in the atomistic region.

critical stress intensities are extremely insensitive to the size of the atomistic region until the very smallest size is reached (see Fig. 7). Even at the smallest size of 45 atoms, the critical stress intensities differ from the larger-size results by only about 3%. At the smallest size, it is evident that the distance from the crack tip to the pad region is almost within the range r_{cut} of the potentials. In addition, the overall deformation along the interface is non-trivial and yet the interface confers no significant errors in the calculation. It should be noted that at the very smallest size, the "detection band" algorithm was turned off so that the very start of crack growth was not misconstrued as dislocation emission by the detection band elements.

These results demonstrate the accuracy of the interface coupling presented in Section 2. In addition, they demonstrate that accurate studies of crack tip phenomena can be achieved using very few atoms, while the finite element region permits the boundary conditions to be applied quite far from the atomistic region. The fact that only a small number of atoms is needed opens up the exciting possibility of using quantum mechanical calculations of the atomistic-scale energetics rather than approximate interatomic potentials. It can be expected that the increase in accuracy in moving from empirical potentials to quantum mechanics will far outweigh the small errors associated with using a small atomistic region in the quantum calculation.

4.2. Nano-indentation

To validate many of the new features contained in the CADD method as described above, we consider a 2D nano-indentation problem for a simple geometry in an FCC Al crystal and compare the results to corresponding fully-atomistic calculations. The geometry of the simulation is shown in Fig. 9. A rigid flat indenter is moved downward into a block of Al oriented such that the vertical (Y) direction coincides with the [110] crystal direction and the out-of-plane (Z) direction lies along the $[1\bar{1}2]$ crystal direction. In this orientation, one of the slip systems of the FCC crystal coincides with the

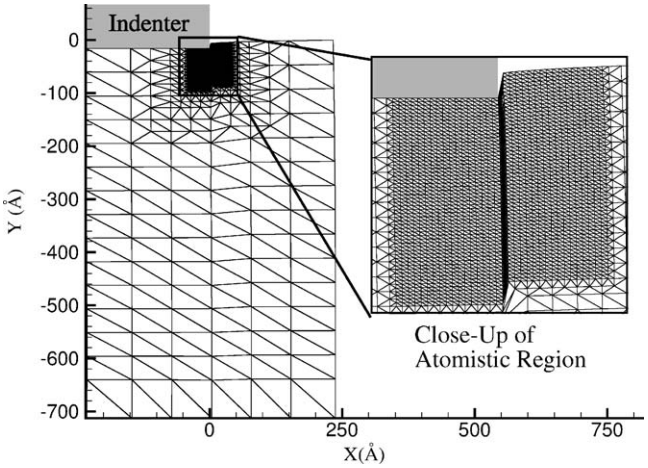

Fig. 9. Model geometry used to simulation indentation into fcc Al by a flat punch. The atomistic region is shown by a mesh joining the atoms to help visualize the slip deformation. Adapted from Shilkrot et al. (2002b).

Y–Z plane and the direction of the punch motion (Y) is parallel to the Burgers vector for this slip system. The rigid punch drives dislocation nucleation, and the emitted dislocations travel downward into the bulk of the material. The size of the system is 713 Å × 466 Å, which permits for a full direct atomistic simulation cell containing 100701 atoms. The CADD simulations contained only 2925 atoms (of which 1046 were pad atoms and therefore not degrees of freedom) and 425 nodes in the finite element mesh.

The EAM potentials of Ercolessi and Adams (1994) are used for the simulation. The boundary conditions on the overall sample were $u_y = 0$ and $T_x = 0$ on the lower edge, $u_y = \delta$ and $u_x = 0$ on the upper edge of the slab under the punch, and traction-free surfaces elsewhere. Here δ is the (downward) displacement of the punch. In the continuum region, the finite element material is anisotropic and linear elastic, with elastic constants that match those produced by the atomistic potentials for an fcc Al crystal in this orientation.[2]

The punch was driven into the material in increments of 0.2 Å. After each increment, equilibrium of the entire system was obtained. At the punch depth of about 9.0 Å, a first pair of partial dislocations was nucleated. A full dislocation was passed to the continuum for each pair of partials detected and the small out-of-plane displacement components of the partials at the atomistic/continuum interface were neglected. The results of the atomistic and CADD simulations are shown in Fig. 10.

[2] The Al potentials used yield fcc elastic constants of $C_{11} = 0.7371$ eV/Å^3, $C_{12} = 0.3888$ eV/Å^3 and $C_{44} = 0.2291$ eV/Å^3. The resulting modulus tensor is appropriately rotated to match the crystal orientation in the atomistic region. The Voigt-average constants used for the dislocation solution are $\mu = 0.2071$ eV/Å^3 and $\lambda = 0.3668$ eV/Å^3.

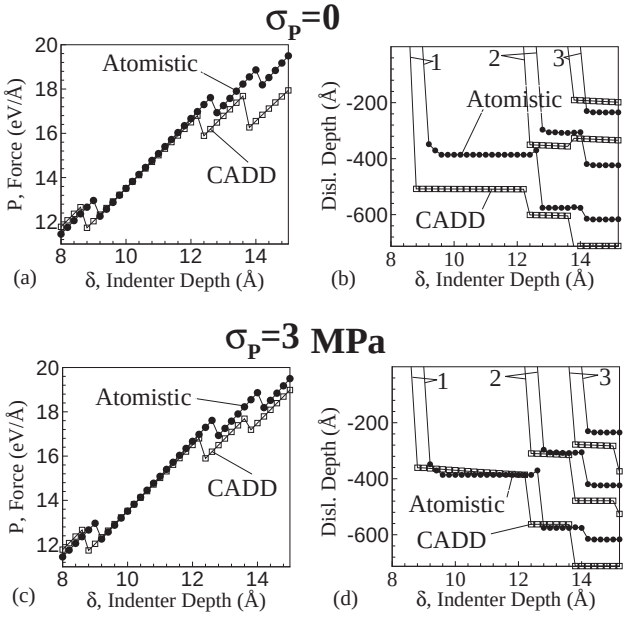

Fig. 10. Comparison between the fully atomistic simulation and the CADD results with two different levels of the Peierls stress, σ_P. The load-displacement curves are shown in (a) and (c), while (b) and (d) show the equilibrium dislocation positions.

Fig. 10(a) shows the load on the punch versus the punch displacement (P–δ); kinks in the curves correspond to points of dislocation emission. The CADD method is in fair agreement with the full atomistics: dislocation emissions occur at slightly earlier load increments, and the loads in CADD are slightly smaller than those in the atomistics at the same punch displacement, i.e. the slope of the CADD curve is lower. We have estimated that more than half of this latter discrepancy is attributed to the non-linear elastic behavior (stiffening under compression) absent in the linear elastic continuum but present in the atomistic material at the large overall strains imposed in deforming this small specimen. In addition, the size of the load drop due to dislocation nucleation is slightly larger in CADD. This is attributable to the greater distances over which the nucleated defects move, as shown in Fig. 10(b). This figure shows the equilibrium positions of the emitted dislocations versus punch depth. The distances travelled by the CADD dislocations are sensitive to the *Peierls stress*, σ_P, in the continuum side of the simulation, which is zero for the results in Figs. 10(a) and (b). In this simulation, the equilibrium position is determined by moving the dislocation to the point where the force due to stresses is zero. Real crystals, as well as the atomistic results to which we are comparing, have a threshold Peierls stress below which dislocations will not move.

It is straightforward to introduce σ_P into CADD, and the above simulations were repeated with $\sigma_P = 3$ MPa (atomistic calculations of this value for fcc Al suggest it is

on the order of 2 MPa Olmsted et al., 2001). The results are shown in Figs. 10(c) and (d), where much better agreement is found with the atomistics. Here, the load drop for each dislocation in the P–δ curve is now very close to that of the atomistic result, and the equilibrium defect positions are considerably closer to the correct ones. Even if the exact Peierls stress value were used, some discrepancy would remain because the potential energy function for a single dislocation in a rather large volume has a very shallow minimum—i.e. there are only small energy differences between widely different positions. Hence, even small errors in the calculation of the continuum force can lead to notable changes in the continuum dislocation position. Simulations carried out for a smaller overall sample size show better agreement because the energy has a sharper minimum in the smaller system. As more dislocations enter the material, the dislocation interactions also sharpen the minimum and the CADD predictions again agree better with the full atomistics. The differences in dislocation positions between Figs. 10(b) and (d) highlight the sensitivity of the results to the numerically obtained stresses: errors in the stresses as small as 3 MPa can lead to considerable differences in the final defect positions.

Finally, the CADD method is meant to augment the mesoscopic discrete dislocation technique by replacing some phenomenological parameters by direct atomistic simulations. The size of systems of real interest may exceed thousands of Å, and small errors in determining the equilibrium dislocation positions are not due to the CADD scheme but rather are intrinsic to the discrete dislocation approach. The errors here are thus acceptable, being within the tolerance of the discrete dislocation method itself.

5. Illustrative examples

Here, we present preliminary results from applications of the CADD model to two more complex deformation problems. The intention of this section is to demonstrate the types of problems for which CADD is suited. More detailed work on these examples, including a thorough analysis and a demonstration of how the CADD results fit with the existing literature will be the subject of future work, with one such study (of nano-indentation) already in press (Shilkrot et al., 2003).

We first consider nanoscale void growth under uniaxial straining of a single crystal. We then study indentation of a single crystal thin film by a cylindrical indenter, which is considerably more rich and complex than the straightforward square-edged indenter used above as a validation problem. As we will show, it is a 2D approximation to a realistic nano-indentation test of the "Brinell" type, i.e., of a spherical-tip indenter, and so is referred to as a "2D Brinell indentation" in what follows.

5.1. Nanometer-scale void growth

The mesh shown previously in Fig. 3 represents the typical mesh dimensions and relative size of the atomistic and continuum regions used to model atomic scale voids. We have considered voids in two different crystals, the first in fcc Ni modeled using

the EAM potentials of Foiles et al. (1986) and the second in an idealized crystal of "hexagonal Ni", i.e. a 2D hexagonal lattice of Ni atoms modeled using the EAM potentials developed for fcc Ni. Before starting the CADD simulations, separate lattice statics calculations were performed to compute the equilibrium lattice constant and elastic moduli for this material.[3] The advantage of studying this idealized crystal is mainly that there are only 6 slip systems, and no partial or screw dislocations will be created. Note that the CADD model is fully capable of handling these types of dislocations (as evidenced in the study of the fcc Ni void), but the hexagonal Ni provides a simpler system to analyze.

In the void simulations, the most important feature of the CADD approach is the ability to *remove* the dislocations from the atomistic region as they are nucleated from the stressed void. In such a deformation, the dislocations want to travel over large distances, and the boundaries in a fully atomistic simulation typically severely limit how far the dislocations can move and thus how much deformation can reliably be obtained. By using CADD, the continuum region acts as a dislocation "sink", isolating the growing void from the effects of the boundaries.

In both simulations, the void is at the center of an atomistic region 200 Å $\times$ 200 Å, embedded at the center of a continuum region approximately 5 μm wide and 6 μm high, as shown in Fig. 3. A uniaxial stress is applied in the y direction by incrementally imposing a uniform strain, holding the y-component of displacement fixed along the top and bottom boundary, and allowing the atoms and continuum to relax. Each incremental strain is superimposed on the relaxed solution from the previous load step to produce a quasi-static loading programme.

In Fig. 11, a series of snapshots of the void in the fcc Ni is shown, focussing on the atomistic region immediately around the void. Snapshots are relaxed configurations at the global applied strain levels indicated. Along the top row of images, a mesh between the atoms is shown, which highlights slip traces as dislocation pass through a region. The bottom row shows the same configurations, but only showing the atoms to reveal the actual deformed void shape and the stacking faults in the Ni lattice. In this case, the void grows by repeated nucleation of dislocations at the left and right corners.

By contrast, a series of images in Fig. 12 shows the deformation of the void in hexagonal Ni. In this case, the images are not in equilibrium, but each is an intermediate configuration assumed by the system during relaxation at an applied strain of $\varepsilon = 0.05$. In this material, we see a type of ductile fracture occurring, whereby the void becomes a crack that advances into the material while occasionally emitting a dislocation from its tip. In both of these simulations, the discrete dislocations that are passed from the atomistic region travel all the way to positions close to the outer boundary of the continuum region, and thus have only long-ranged elastic effects on the subsequent deformation near the atomic-scale void.

[3] Lattice constant, $a_0 = 2.43$ Å, in-plane elastic constants $C_{11} = C_{22} = 1.842$ eV/Å^3, $C_{12} = \lambda = 0.8959$ eV/Å^3, $C_{66} = \mu = 0.4729$ eV/Å^3.

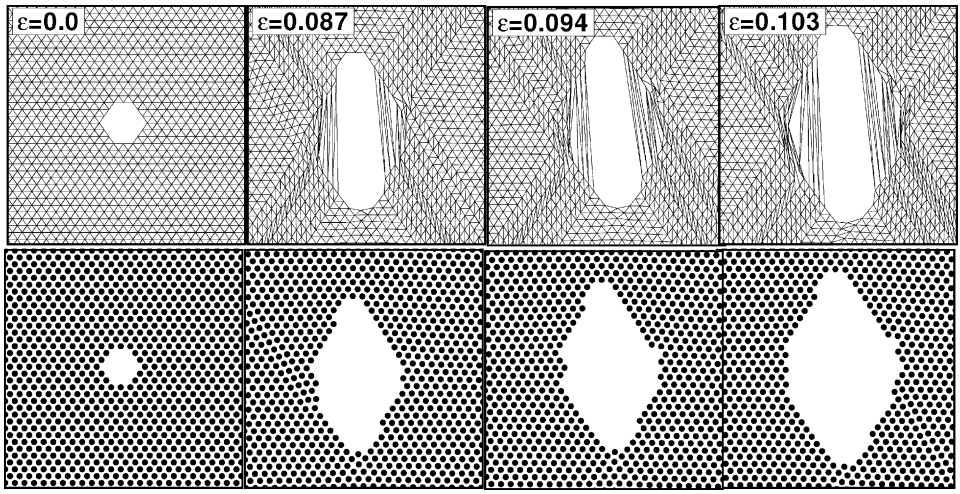

Fig. 11. Close-up of the atomistic region around a void in fcc Ni. The void grows by repeated dislocation nucleation at the right and left corners. Top row shows a mesh joining the atoms to visualize the slip deformation, bottom row shows only the atoms.

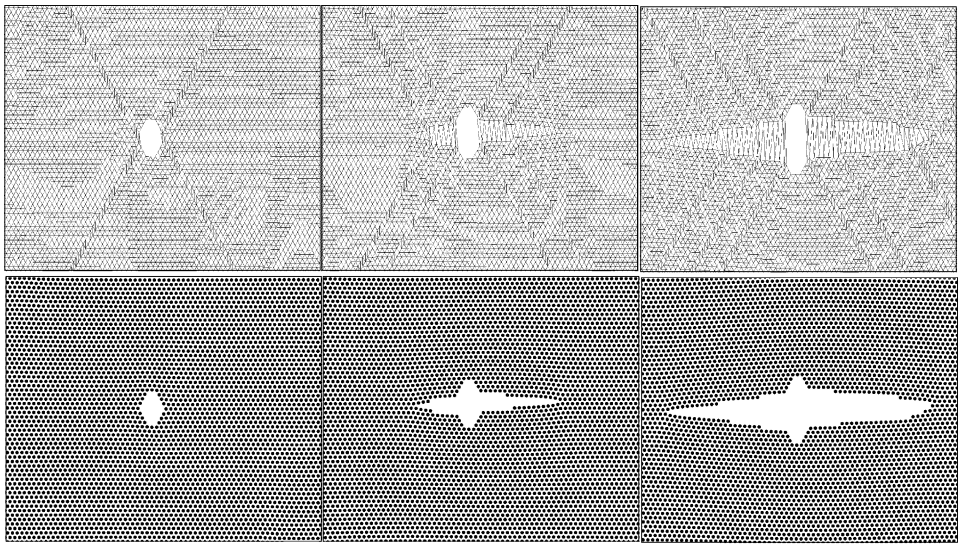

Fig. 12. Close-up of the atomistic region around a void in hexagonal Ni. The void serves as a nucleation site for a crack, which grows while occasionally emitting dislocations from its tip. Top row shows a mesh joining the atoms to visualize the slip deformation, bottom row shows only the atoms.

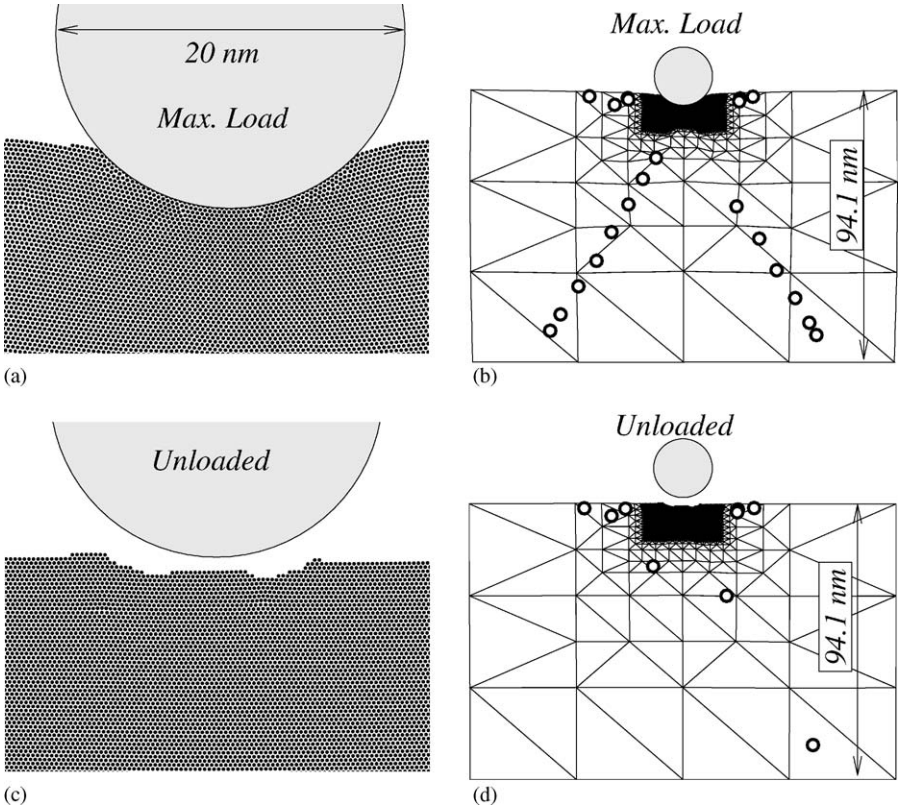

Fig. 13. Configuration of the atomic region ((a) and (c)) and positions of the discrete dislocations ((b) and (d)) at maximum load ((a)–(b)) and after full unloading ((c)–(d)) for the displacement-controlled indentation of single crystal.

5.2. "Brinell" nano-indentation

In this simulation, a rigid, frictionless cylindrical indenter with radius $R = 100$ Å is modeled as a repulsive potential. The potential interacts with the atoms and forces them to remain outside the 100 Å radius of the indenter.

The material to be indented is a thin film of single crystal hexagonal Al (as described in Section 4), with a bottom surface bonded to a rigid substrate and an free upper surface into which the indenter is pressed. The model mesh is shown in Fig. 13(b). Loading is quasi-static, and simulates a *displacement-controlled* nano-indentation experiment by incrementally moving the indenter down and superimposing a uniform compressive strain on the equilibrium solution from the previous load step. The atoms and nodes are then relaxed while holding the indenter fixed. The indenter was moved by 2 Å increments to a maximum penetration of 58 Å, and then unloaded, again using 2 Å steps.

Fig. 13 shows the atomistic region and the entire model at both the maximum load and after unloading. Open circles show the locations of the discrete dislocations. Dislocations nucleate as dipoles within the atomistic region, below the surface of the crystal and move along the slip planes oriented at $\pm 30^\circ$ to the vertical. One member of each dipole pair travels up to the surface, where is reflects back into the crystal and leaves a residual dislocation on the surface. The reflected defects ultimately dissociate onto the horizontal slip planes and move to the left and right of the atomistic region. The second member of each dipole travels down into the continuum, and ultimately runs up against the rigid lower boundary of the model. The resulting pile-up of dislocations is clear in Fig. 13(b). Upon unloading, many dislocations remain in the crystal, resulting in a permanent impression on the surface after unloading, as shown in Figs. 13(c) and (d).

In a detailed study of this simulation (Shilkrot et al., 2003), we examine the deformation mechanisms under the indenter in detail, and correlate them with features in the load-displacement curve. We also observe an indentation size effect, wherein the apparent hardness of the crystal decreases with increasing indentation depth.

6. Discussion and conclusions

We have presented the details of a coupled atomistic and continuum method which is capable of supporting discrete dislocations in the continuum region. In addition, the method includes algorithms to automatically detect dislocations as they want to move across the atomistic/continuum interface, and correctly converts dislocations between the two domains.

The coupling scheme that we have used follows closely that of Kohlhoff et al. (1991), and has been demonstrated by Curtin and Miller (2003) to be the most accurate coupling scheme devised to date. By accurate, we specifically mean that there are no spurious "ghost" forces or relaxations at the interface. This important advantage of the coupling approach comes at the expense of no longer having a well-defined energy functional, and some reduction in convergence rates.

The CADD method simultaneously extends the realm of applicability of both fully atomistic simulations and discrete dislocation approaches. For atomistic methods, CADD allows for larger systems to be studied without the need to explicitly treat every atom in the problem. While other coupled methods can provide similar benefit, CADD is well-suited to problems where dislocations want to travel over long distances. This is often the case in ductile metals with high dislocation mobility and low Peierls barriers. In such materials, atomistic simulations of fracture, grain boundary deformation, void growth and indentation are often limited by the dislocations reaching the boundaries of the simulation box. CADD extends the size of the simulation to macroscopic length scales, serving as a dislocation sink and isolating the atomistic region from simulation boundary artifacts. On the other hand, CADD extends the range of problems accessible to discrete dislocation methods by reducing the dependence on phenomenological rules for dislocation nucleation. Critical regions, for example at crack tips, inclusions or grain boundaries, can be modeled fully atomistically to ensure that nucleation is controlled only by interatomic forces.

We have used two validation problems to test the method and quantify the errors introduced. First, we computed the critical stress intensity factors for advance and recession of an atomically sharp crack in a single crystal. We found that excellent accuracy could be obtained with an atomistic region around the crack tip containing as few as 45 atoms. This is a promising result for future efforts to extend CADD to include tight-binding or other more sophisticated atomistic models, since the computational effort of such techniques is orders of magnitude greater than that for empirical potentials. Our second validation example was a direct comparison between a fully atomistic simulation and a CADD simulation of indentation by a flat punch. Here, we observed that the main errors in the CADD method arise from a lack of a well-defined Peierls stress in the continuum region, and the sensitivity of highly mobile dislocations to small errors in the numerically computed stresses. For the types of applications envisioned for the CADD method, these errors are no worse than those introduced by the discrete dislocation formalism itself in the continuum region.

Two examples of CADD simulations, of atomic scale void growth and "Brinell" indentation by a spherical indenter, were presented briefly and will be the subject of detailed studies in future publications. In the void growth simulations, the main advantage of CADD is the ability to carry the dislocations far from the region of interest around the void while maintaining the correct backstress from the defects. The Brinell indentation example is studied in detail in another article (Shilkrot et al., 2003).

It is noted above that the method is currently designed for two-dimensional, quasi-static problems. Extensions of the model to dynamics and 3D are believed to be possible and will be the focus of future work. In the case of dynamics, the extension is believed to be straightforward in a formal sense, but lessons taken from methods like the CLS approach mentioned earlier have shown the need for careful treatment of the atomistic/continuum interface region to avoid non-physical wave reflections during the simulation (Broughton et al., 1999; Rudd and Broughton, 1998, 2000). A 3D version of the CADD method is definitely more conceptually difficult, but recent progress with three-dimensional DD simulations (Weygand et al., 2002) may be applicable to future developments of a 3D CADD model. The main difficulty is that, unlike the situation in 2D where a dislocation is effectively a "point" residing unambiguously in either the atomistic or the continuum region, a 3D dislocation is a loop that will often extend across the atomistic/continuum interface. The challenge, then, will be in devising a scheme to effect a transition from an atomistic to a continuum description of a single continuous dislocation loop.

Another important future direction for CADD is an implementation suitable for parallel computing. The way in which CADD naturally decouples the atomistic and continuum regions makes it well-suited to parallelization, effectively allowing the use of previously established tools for parallelization of atomistic and DD methods.

Acknowledgements

The authors gratefully acknowledge support of this work by the US Air Force Office of Scientific Research, Grant #F49620-99-1-0272, under the MURI program entitled

"Virtual Design and Testing of Materials: a Multiscale Approach" at Brown University. RM also thanks the NSERC of Canada for finanical support. Finally, the authors thank Dr. Vijay Shastry for help the simulations of brittle crack growth and Professors Alan Needleman and Rob Phillips for useful conversations during the course of this work.

Appendix

In this appendix, we derive the expression for the energy E^{c} of the continuum region of the material that is used in computing the P–K forces acting on the dislocations. As described in Section 2.2, elastic fields in the continuum are partitioned into the $\tilde{}$ component associated with the fields of the dislocations in an infinite linearly elastic material and the $\hat{}$ component required to satisfy boundary conditions applied on the external boundary $\partial\Omega_C$ and the interface $\partial\Omega_I$. Using this partition explicitly, the expression for the energy E^{c} is written as:

$$E^{\mathrm{c}} = \frac{1}{2}\int_{\Omega_C} (\hat{\boldsymbol{\sigma}} + \tilde{\boldsymbol{\sigma}}) : (\hat{\boldsymbol{\varepsilon}} + \tilde{\boldsymbol{\varepsilon}})\,\mathrm{d}V - \int_{\partial\Omega_T} \boldsymbol{T}_0(\tilde{\boldsymbol{u}} + \hat{\boldsymbol{u}})\,\mathrm{d}A, \tag{A.1}$$

where the integrals over the continuum region and its boundary are two and one dimensional respectively. The first integral in Eq. (A.1) is simply the stored elastic energy of the continuum region whereas the second integral represents the potential energy of applied external tractions.

Expanding the integrals, we encounter the terms

$$\frac{1}{2}\int_{\Omega_C} \tilde{\boldsymbol{\sigma}} : \hat{\boldsymbol{\varepsilon}}\,\mathrm{d}V + \frac{1}{2}\int_{\Omega_C} \hat{\boldsymbol{\sigma}} : \tilde{\boldsymbol{\varepsilon}}\,\mathrm{d}V, \tag{A.2}$$

which are equal by virtue of the reciprocal theorem. Further we can use the principle of virtual work to rewrite these terms as an integral over the boundary of the continuum region:

$$\int_{\Omega_C} \tilde{\boldsymbol{\sigma}} : \hat{\boldsymbol{\varepsilon}}\,\mathrm{d}V = \int_{\partial\Omega_C+\partial\Omega_I} (\tilde{\boldsymbol{\sigma}}\boldsymbol{n})\hat{\boldsymbol{u}}\,\mathrm{d}A, \tag{A.3}$$

where $\boldsymbol{n}$ is the outer normal to the boundary of the continuum region. In Section 2.2 the product $\tilde{\boldsymbol{\sigma}}\boldsymbol{n}$ is denoted as $\tilde{\boldsymbol{T}}$. Note that although the field $\tilde{\boldsymbol{\sigma}}$ is singular, all singularities in Eq. (A.3) are integrated out in the surface integral. The field $\tilde{\boldsymbol{T}}$ is, in turn, continuous on the boundary $\partial\Omega_C + \partial\Omega_I$ as is the field $\hat{\boldsymbol{u}}$.

With this simplification, Eq. (A.1) becomes

$$E^{\mathrm{c}} = \frac{1}{2}\int_{\Omega_C} \hat{\boldsymbol{\sigma}} : \hat{\boldsymbol{\varepsilon}}\,\mathrm{d}V + \frac{1}{2}\int_{\Omega_C} \tilde{\boldsymbol{\sigma}} : \tilde{\boldsymbol{\varepsilon}}\,\mathrm{d}V - \int_{\partial\Omega_T} \boldsymbol{T}_0(\tilde{\boldsymbol{u}} + \hat{\boldsymbol{u}})\,\mathrm{d}A + \int_{\partial\Omega_T} \tilde{\boldsymbol{T}}\hat{\boldsymbol{u}}\,\mathrm{d}A. \tag{A.4}$$

Note that the last integral, which comes from the principal of virtual work, is strictly over the entire boundary on the continuum region, $\partial\Omega_C + \partial\Omega_I$. However, the interface $\partial\Omega_I$ is a displacement boundary condition, and so the only non-zero contribution is from the traction boundaries $\partial\Omega_T$.

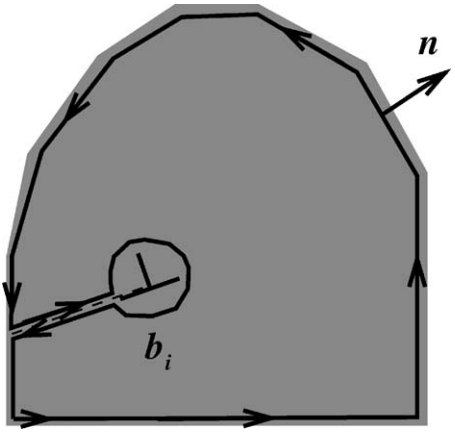

Fig. 14. Contour of integration, L_i, used for dislocation i in the computation of elastic energy of the continuum region.

We consider separately each term in Eq. (A.4). The first term involving the product of two $\hat{}$ fields is the easiest to compute. After the displacement field $\hat{\boldsymbol{u}}$ is discretized in order to apply the finite element technique, the integral simply becomes the finite element elastic energy (Zienkiewicz, 1991) that is routinely obtained in the finite element method. Expressed in terms of the vector of the discretized displacement field $\hat{\boldsymbol{u}}_C$ and $\hat{\boldsymbol{u}}_I$ (the subscripts C and I indicate the "continuum" and "interface" nodes, respectively) the integral becomes the convolution of the finite element stiffness matrix, $\boldsymbol{C}$, of the continuum region and the vectors $\hat{\boldsymbol{u}}_C$ and $\hat{\boldsymbol{u}}_I$

$$\frac{1}{2}\int_{\Omega_C} \hat{\boldsymbol{\sigma}} : \hat{\boldsymbol{\varepsilon}}\,\mathrm{d}V = \frac{1}{2}(\hat{\boldsymbol{u}}_C \cdot \boldsymbol{C}_{CC} \cdot \hat{\boldsymbol{u}}_C + \hat{\boldsymbol{u}}_I \cdot \boldsymbol{C}_{II} \cdot \hat{\boldsymbol{u}}_I) + \hat{\boldsymbol{u}}_C \cdot \boldsymbol{C}_{CI} \cdot \hat{\boldsymbol{u}}_I, \tag{A.5}$$

where $\boldsymbol{C}_{CC}$, $\boldsymbol{C}_{II}$, $\boldsymbol{C}_{CI}$ represent the FEM stiffness matrices coupling the various nodal displacements.

The next integral involving the product of $\tilde{}$ fields requires special consideration because a dislocation displacement field is multivalued and singular. Expressing the integral as a sum of contributions from individual dislocations yields:

$$\frac{1}{2}\int_{\Omega_C} \tilde{\boldsymbol{\sigma}} : \tilde{\boldsymbol{\varepsilon}}\,\mathrm{d}V = \frac{1}{2}\sum_{l\neq m}\int_{\Omega_C} \tilde{\boldsymbol{\sigma}}^l : \tilde{\boldsymbol{\varepsilon}}^m\,\mathrm{d}V + \frac{1}{2}\sum_{l}\int_{\Omega_C} \tilde{\boldsymbol{\sigma}}^l : \tilde{\boldsymbol{\varepsilon}}^l\,\mathrm{d}V, \tag{A.6}$$

where we separate terms involving two different dislocations and contributions from individual dislocations.

To make a multivalued displacement field of an isolated dislocation single-valued, one introduces a semi-infinite cut in the plane starting at the dislocation position (Hirth and Lothe, 1992). In order to reduce the surface integrals in Eq. (A.6) to line integrals, for dislocation i we define a contour L_i of integration shown in Fig. 14. Each contour consists of the boundary of the continuum region $\partial\Omega_C + \partial\Omega_I$, a small circle around the singular dislocation core and two segments along the cut in the dislocation field that extend from the core to the boundary of the continuum region. Application of

the principle of virtual work to the integrals inside the summation signs in Eq. (A.6) yields (for the term involving dislocations l and m):

$$\int_{\Omega_C} \tilde{\boldsymbol{\sigma}}^l : \tilde{\boldsymbol{\varepsilon}}^m \, \mathrm{d}V = \int_{L_m} \tilde{\boldsymbol{\sigma}}^l_{ij} \tilde{\boldsymbol{u}}^m_i \boldsymbol{n}_j \, \mathrm{d}A, \tag{A.7}$$

where vector $\boldsymbol{n}$ is the outer unit normal to the contour L_m and parameter s is a scalar length along the contour of integration. The contour is oriented in the counterclockwise direction.

We restrict our consideration to edge dislocation only with the z-component of the displacement equal to zero. Since in our formulation elastic fields of dislocations are considered isotropic, the components of the stress produced by an individual edge dislocation can be expressed in terms of the derivatives of the readily available Airy stress function χ (Hirth and Lothe, 1992):

$$\tilde{\boldsymbol{\sigma}}_{xx} = \frac{\partial^2 \chi}{\partial^2 y}, \quad \tilde{\boldsymbol{\sigma}}_{yy} = \frac{\partial^2 \chi}{\partial^2 x}, \quad \tilde{\boldsymbol{\sigma}}_{xy} = -\frac{\partial^2 \chi}{\partial y \partial x}, \tag{A.8}$$

where for a dislocation with a Burgers vector $\boldsymbol{b}$ the stress function is

$$\chi = \frac{\mu}{4\pi(1-\nu)} (b_y x - b_x y) \log(r). \tag{A.9}$$

Here μ and ν are the shear modulus and Poisson's ration of the material.

Using the representation of the stresses in terms of derivatives of the Airy stress function the line integral can be computed by parts. Since all contours L are closed and the function inside the sign of integral is single-valued on those contours, the integration yields

$$\int_{L_m} \tilde{\boldsymbol{\sigma}}^l_{ij} \tilde{\boldsymbol{u}}^m_i \boldsymbol{n}_j \, \mathrm{d}A = -\int_{L_m} \left(\frac{\partial \chi^l}{\partial y} \nabla \tilde{u}^m_y - \frac{\partial \chi^l}{\partial x} \nabla \tilde{u}^m_x \right) \mathrm{d}\boldsymbol{s}, \tag{A.10}$$

where $\mathrm{d}\boldsymbol{s}$ is a vector element of contour length. Unlike the functions $\tilde{\boldsymbol{u}}$, the derivatives of $\tilde{\boldsymbol{u}}$ are single-valued. Hence, the integral along the segments of the cut cancel each other out and the integral needs to be computed only over the boundary of the continuum region and the small circle around the dislocation core. The latter integral can be easily evaluated for cases when $m \neq l$:

$$-\int_{L_m} \left(\frac{\partial \chi^l}{\partial y} \nabla \tilde{u}^m_y - \frac{\partial \chi^l}{\partial x} \nabla \tilde{u}^m_x \right) \mathrm{d}\boldsymbol{s} = -\int_{\partial\Omega_C + \partial\Omega_I} \left(\frac{\partial \chi^l}{\partial y} \nabla \tilde{u}^m_y - \frac{\partial \chi^l}{\partial x} \nabla \tilde{u}^m_x \right) \mathrm{d}\boldsymbol{s} + \left(\frac{\partial \chi^l}{\partial y} b^m_x - \frac{\partial \chi^l}{\partial x} b^m_y \right), \tag{A.11}$$

where $\boldsymbol{b}^m$ is the Burgers vector of dislocation m. If $m = l$ then the integral around the dislocation core is singular. However, it can be omitted because the expression for E^c is not needed by itself but only its variation with respect to positions of dislocations in the continuum region.

Assembling the terms from Eqs. (A.11) and (A.5) into Eq. (A.4) we derive the equation for the energy of the continuum region as

$$E^{c} = \frac{1}{2}(\hat{\boldsymbol{u}}_C \cdot \boldsymbol{C}_{CC} \cdot \hat{\boldsymbol{u}}_C + \hat{\boldsymbol{u}}_I \cdot \boldsymbol{C}_{II} \cdot \hat{\boldsymbol{u}}_I) + \hat{\boldsymbol{u}}_C \cdot \boldsymbol{C}_{CI} \cdot \hat{\boldsymbol{u}}_I + \frac{1}{2}\sum_{l \neq m}\left(\frac{\partial \chi^l}{\partial y} b_x^m - \frac{\partial \chi^l}{\partial x} b_y^m\right) - \frac{1}{2}\int_{\partial\Omega_C + \partial\Omega_I}\left(\frac{\partial \chi}{\partial y}\nabla \tilde{u}_y - \frac{\partial \chi}{\partial x}\nabla \tilde{u}_x\right) \mathrm{d}\boldsymbol{A} - \int_{\partial\Omega_T} \boldsymbol{T}_0(\tilde{\boldsymbol{u}} + \hat{\boldsymbol{u}})\,\mathrm{d}A + \int_{\partial\Omega_T} \tilde{\boldsymbol{T}}\hat{\boldsymbol{u}}\,\mathrm{d}A. \tag{A.12}$$

Here χ is the stress function of the dislocation field that is equal to the sum of the stress functions of individual dislocations. The line integrals entering this expression are computed using the standard finite element integration scheme of Gaussian quadrature. Special care must be taken in dealing with the last term in the presence of discontinuities in the dislocation displacement field $\tilde{\boldsymbol{u}}$ (dislocation slip steps) on $\partial\Omega_T$. In this case one should explicitly keep track of these discontinuities and add appropriate terms to the value of the integral.

The final step is to treat all continuum tractions via their discretized nodal forces, to facilitate the rapid calculation of the final two integrals in the energy expression. The final discretized continuum energy is then

$$E^{c} = \frac{1}{2}(\hat{\boldsymbol{u}}_C \cdot \boldsymbol{C}_{CC} \cdot \hat{\boldsymbol{u}}_C + \hat{\boldsymbol{u}}_I \cdot \boldsymbol{C}_{II} \cdot \hat{\boldsymbol{u}}_I) + \hat{\boldsymbol{u}}_C \cdot \boldsymbol{C}_{CI} \cdot \hat{\boldsymbol{u}}_I + \frac{1}{2}\sum_{l \neq m}\left(\frac{\partial \chi^l}{\partial y} b_x^m - \frac{\partial \chi^l}{\partial x} b_y^m\right) - \frac{1}{2}\int_{\partial\Omega_C + \partial\Omega_I}\left(\frac{\partial \chi}{\partial y}\nabla \tilde{u}_y - \frac{\partial \chi}{\partial x}\nabla \tilde{u}_x\right) \mathrm{d}\boldsymbol{A} - \boldsymbol{t}_0 \cdot (\tilde{\boldsymbol{u}}_C + \hat{\boldsymbol{u}}_C) + \tilde{\boldsymbol{t}}_C \cdot \hat{\boldsymbol{u}}_C, \tag{A.13}$$

where the lower case $\boldsymbol{t}$ represents a nodal force vector.

References

Abraham, F.F., Walkup, R., Gao, H.J., Duchaineau, M., De la Rubia, T.D., Seager, M., 2002. Simulating materials failure by using up to one billion atoms and the world's fastest computer: brittle fracture. Proc. Natl. Acad. Sci. USA 99 (9), 5777–5782.

Broughton, J.Q., Abraham, F.F., Bernstein, N., Kaxiras, E., 1999. Concurrent coupling of length scales: methodology and application. Phys. Rev. B 60 (4), 2391–2403.

Curtin, W.A., Miller, R.E., 2003. Atomistic/continuum coupling in computational materials science. Model. Simul. Mater. Sci. Eng. 11 (3), R33–R68.

Daw, M.S., Baskes, M.I., 1984. Embedded-atom method: derivation and application to impurities, surfaces, and other defects in metals. Phys. Rev. B 29, 6443–6453.

Ercolessi, F., Adams, J.B., 1994. Interatomic potentials from first-principles calculations—the force-matching method. Europhys. Lett. 26, 583.

Foiles, S.M., Baskes, M.I., Daw, M.S., 1986. Embedded-atom-method functions for the fcc metals Cu, Ag, Au, Ni, Pd, Pt and their alloys. Phys. Rev. B 33, 7983–7991.

Gumbsch, P., Beltz, G.E., 1995. On the continuum versus atomistic descriptions of dislocation nucleation and cleavage in nickel. Model. Simul. Mater. Sci. Eng. 3 (5), 597–613.

Hirth, J.P., Lothe, J., 1992. Theory of Dislocations. Krieger, Malabar, Florida.
Kohlhoff, S., Gumbsch, P., Fischmeister, H.F., 1991. Crack propagation in bcc crystals studied with a combined finite-element and atomistic model. Philos. Mag. A 64 (4), 851–878.
Kubin, L.P., Canova, G., 1992. The modelling of dislocation patterns. Scripta Met. 27, 957–962.
Olmsted, D.L., Hardikar, K.Y., Phillips, R., 2001. Lattice resistance and peierls stress in finite size atomistic dislocation simulations. Model. Simul. Mater. Sci. Eng. 9, 215.
Press, W.H., Teukolsky, S.A., Vetterling, W.T., Flannery, B.P., 1992. Numerical Recipes in FORTRAN: The Art of Scientific Computing, 2nd Edition. Cambridge University Press, Cambridge.
Rudd, R.E., Broughton, J.Q., 1998. Coarse-grained molecular dynamics and the atomic limit of finite elements. Phys. Rev. B 58 (10), R5893–R5896.
Rudd, R.E., Broughton, J.Q., 2000. Concurrent coupling of length scales in solid state systems. Phys. Status Solidi B 217, 251–291.
Shenoy, V.B., Miller, R., Tadmor, E.B., Phillips, R., Ortiz, M., 1998. Quasicontinuum models of interfacial structure and deformation. Phys. Rev. Lett. 80 (4), 742–745.
Shenoy, V.B., Kukta, R.V., Phillips, R., 2000. Mesoscopic analysis of structure and strength of dislocation junctions in fcc metals. Phys. Rev. Lett. 84 (7), 1491–1494.
Shilkrot, L.E., Curtin, W.A., Miller, R.E., 2002a. A coupled atomistic/continuum model of defects in solids. J. Mech. Phys. Sol. 50, 2085–2106.
Shilkrot, L.E., Miller, R.E., Curtin, W.A., 2002b. Coupled atomistic and discrete dislocation plasticity, Phys. Rev. Lett. 89 (2), 025501–1–025501–4.
Shilkrot, L.E., Miller, R.E., Curtin, W.A., 2003. A coupled atomistics and discrete dislocation plasticity simulation of nano-indentation into single crystal thin films. Acta Mat. in press.
Tadmor, E.B., Ortiz, M., Phillips, R., 1996. Quasicontinuum analysis of defects in solids. Philos. Mag. A 73 (6), 1529–1563.
van der Giessen, E., Needleman, A., 1995. Discrete dislocation plasticity: a simple planar model. Model. Simul. Mater. Sci. Eng. 3, 689–735.
Vitek, V., 1974. Theory of the core structures of dislocations in body-centred-cubic metals. Cryst. Lattice Defects 5, 1–34.
Wei Yang, Honglai Tan, Tianfu Guo, 1994. Evolution of crack tip processes. Model. Simul. Mater. Sci. Eng. 2, 767–782.
Weygand, D., Friedman, L.H., van der Giessen, E., Needleman, A., 2002. Aspects of boundary-value problem solutions with three-dimensional dislocation dynamics. Model. Simul. Mater. Sci. Eng. 10 (4), 437–468.
Zbib, H.M., Rhee, M., Hirth, J.P., 1998. On plastic deformation and the dynamics of 3D dislocations. Int. J. Mech. Sci. 40, 113–127.
Zienkiewicz, O.C., 1991. The Finite Element Method, Vol. 1–2, 4th Edition. McGraw-Hill, London.
Zimmerman, J.A., Kelchner, C.L., Klein, P.A., Hamilton, J.C., Foiles, S.M., 2001. Surface step effects on nanoindentation, Phys. Rev. Lett. 87 (16) 165507-1–165507-4.